Hematite Decorated MWCNT Nanohybrids: A Facile Synthesis

Sajid Hussain*, S. F. Hasany and Syed Usman Ali
[1,2,3]*NED University of Engineering and Technology, Karachi Pakistan.*
sajid@iiee.edu.pk

(Received on 20th April 2022, accepted in revised form 10th June 2022)

Summary: Hybrid nanomaterials with different sizes, shapes, compositions, and morphology have gained importance for numerous physicochemical, electrical and magnetic acumens. Multi-Walled Carbon nanotubes (MWCNTs) can be decorated with various metals to produce nanohybrids to attain desired features for leading high-tech applications. The presented research work comprises a cost- effective wet chemical method to fabricate Hematite based (α-Fe_2O_3- MWCNTs) nanohybrids. Physicochemical characteristics were studied by XRD, FTIR, SEM and VSM, and EDX, respectively. Results showed well-decorated hematite nanocrystals (size ~ 26nm) on the surface of MWCNTs. Magnetic behaviors exhibited a ferromagnetic material with saturation and remnant magnetization and coercivity of ~ 1.2 emu/g, 0.5 emu/g and 200 Oersted respectively, which makes it a suitable contender in advanced energy storage devices.

Keywords: Nanohybrids, Facile synthesis, Hematite, MWCNT.

Introduction

Metal oxide nanoparticles are of undue importance in wide-scale sensor fabrications[1, 2], nanogenerator devices[3], Lithium-Ion batteries[4] and major catalysis activities[3], respectively. The preparation methods play a key role in the obtainment of specific particle size; shape and for explicit surface chemistry and engineering applications. Wet Chemical techniques are the facile route to attain desired nanoparticles with good control over size, shape, and phase in comparison to other techniques[5].

Hematite(α-Fe_2O_3), the most abundant and stable polymorph of iron oxide on Earth crust[1, 3], has wide application at micro and nanoscale in saleable and industrial applications due to nontoxic, low cost, corrosion resistance and environmentally friendly behaviors[4-6]. Resistance and environmental compatibility[4-6].

Carbon nanotubes (CNTs) exhibit a high aspect ratio[7], with a well-developed mesoporous structure[8-10] that contributes to superior behaviors when nanohybrids of Metal-CNTs are tailored [11, 12]. Nanohybrids connect the power of nanotechnology[13] and engineered targeting to enable improved and non-invasive wide spectrum applications. CNTs have proved excellent electrochemical and magnetic outturn in hybrids with nano-sized Fe_2O_3 due to synergetic partnership among them [14] synthesized a CNT-Fe_2O_3 carbon composite and demonstrated a capacitance of 787.5 F g^{-1} with high cyclic stability[15].

The goal of presented study is to investigate a cost-effective fabrication method of hematite–MWCNTs nanohybrids, largely due to the higher stability of hematite over other polymorphs of iron oxide [16], and high-tech applications. The designed method can be used to make a wide range of sophisticated materials with well-controlled structures for a variety of applications in bulk, such as optical and electronic biomaterials, materials, sensing, catalysis, coating, and energy storage devices[17].

Experimental

Experimental Materials

All of the chemicals utilized were of the highest quality. Sigma–Aldrich provided nitric acid, iron nitrate [$Fe(NO_3)_3 9H_2O$), hydrochloric acid, ammonium hydroxide, and sodium hydroxide. Merck provided the lead nitrate (Germany). The MWCNTs employed in this work are 92 percent pure, with an exterior diameter of 30–50 nm, an interior diameter of 5–10 nm, and a length of 10–20 mm (Chengdu Organic Chemicals, China).

Experimental Method

Primarily, MWCNT was surface activated to establish oxygen bridge in between components of Hematite and MWCNT nanohybrids. Calculated amount of raw MWCNT was added to the reaction vessel of 1 M solution of concentrated nitric acid (HNO_3) for 6(six) hours contact time at a temperature condition of 60 ^{o} C. Activated MWCNT was washed

*To whom all correspondence should be addressed.

and filtered by deionized water until the pH becomes neutral.; dried at 100 ° C, finally.

In the next stage, a calculated amount of Iron nitrate nonahydrate Fe $(NO_3)_3.9H_2O$ was mechanically stirred at high speed for one hour under the nitrogen environment. 1:2 ratio of ammonium hydroxide was added dropwise in iron precursor to attain supersaturated conditions. Later, nitrogen bubbled water was poured into the reaction vessel and stirred for ten min to complete reaction. Finally, calculated amount of surface-activated MWCNT was added to the reaction vessel and stirred at high speed under the nitrogen environment for one hour.

The solution obtained was washed, centrifuged with distilled water and ethanol (3 X 10 ml) times, respectively. The obtained product was left overnight in the ethanol environment to control the diffusion-based growth of Iron hydroxide nuclei. Furnace treatment was performed at 500 ° C for 15 min to achieve well developed nanocrystals of Hematite decorated on MWCNTs.

Results and Discussion

X-Ray Diffraction (XRD) analysis

The synthesized nanohybrid samples were characterized by XRD for their crystallinity, phase, and composition. Fig. 1 shows the XRD analysis of the synthesized composite using an XRD diffractometer (XPERTPRO) with Cu K having a wavelength (= 1.5416 A°) and operating at 30 mA and 40K volt, with vertical lines representing Reference Data Indexed (COD: 901-2231) and (COD:101-1241) for MWCNT and Hematite, respectively.

The produced composite could be indexed for MWCNT or Hematite, and the XRD spectra revealed multiple peaks, indicating a nanohybrid[18] at peaks at 26°, 44.5°, and 77° theta [16]. The cylindrical and Multi-walled nature of graphene sheets with an interlayer spacing of 0.31 nm, 0.21 nm, and 0.122 nm, confirmed CNT existence [19] (P_{4132}, ICDD: 391346), while remaining peaks at 41°, 37°, 64°, 72°, and 77° theta values correspond to 0.232 nm, 0.212 nm (P4132, ICDD: 391346). The average crystallite size was calculated by Debye–Scherer Equation, which in this case was 0.455 nm using the Debye– Scherer formula $D=0.9\lambda / \beta Cos\theta$, where *'λ'* is the wavelength (0.154 nm), *'β'* is the angular line width at half maximum intensity in radians, and *'θ'* is the Bragg's angle. The parameters obtained with 2θ and intensity from XRD are listed in

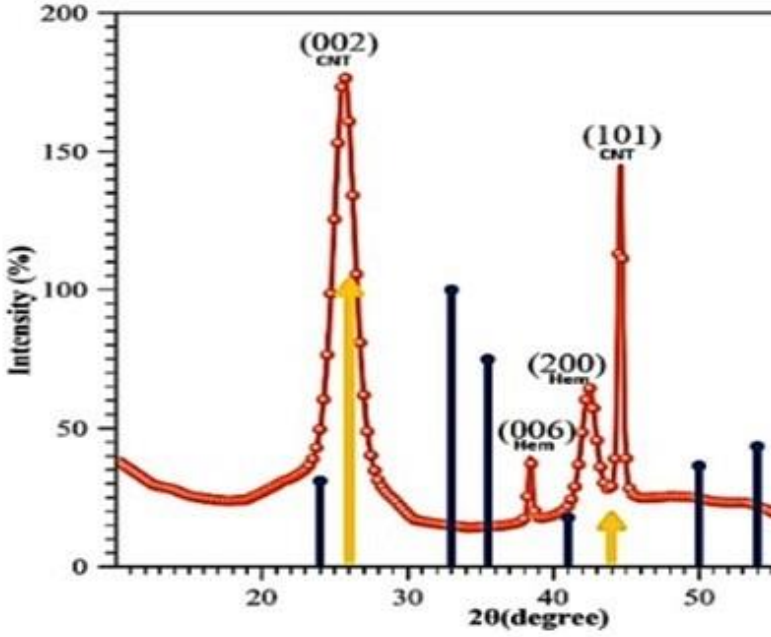

Fig. *1*: XRD diffractogram of Hematite – MWCNT.

Table-*1* below.

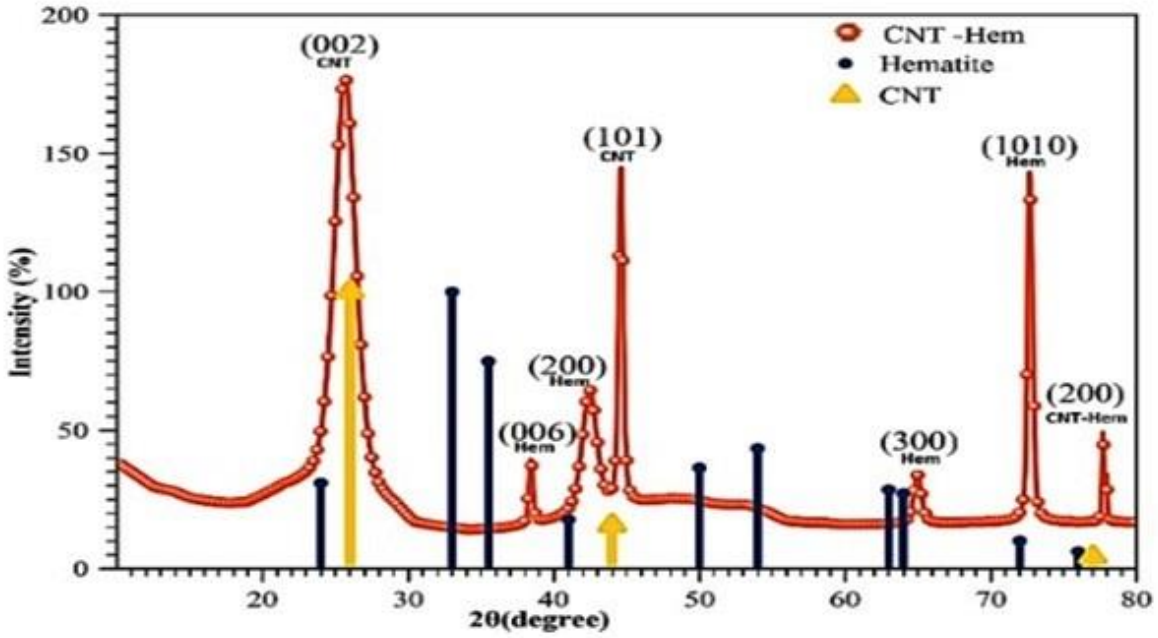

Fig. 1: XRD diffractogram of Hematite – MWCNT.

Table-1: Presenting different values obtained by XRD analysis.

2θ (degree)	FWHW (radian)	D Spacing (nm)	Intensity (%)	Wavelength λ(A°)	Crystal Size D(nm)	Average Crystal Size (nm)
38.39708	0.0051	0.234440	15.28	1.54	28.485	26.233
44.57388	0.0060	0.203282	80.32	1.54	24.919	
64.91269	0.0103	0.143655	11.47	1.54	24.919	
72.64859	0.0051	0.130148	100.00	1.54	33.389	

The anisotropic crystallite size was determined by the width of the peaks in the diffraction spectra, which includes sharp and wide peaks, demonstrating heterogeneous crystallite sizes in the synthesized nanohybrid. The strong peaks at 37.3°, 43.5°, 73.5°, and 76.6° are due to most crystalline crystals, whereas less ordered crystals can be found at 24.5°, 43.4°, and 64° [20]. The resulting peaks were pushed toward higher 2 values, indicating that the interlayer spacing is narrower than the hematite reference peaks [16]. Some peaks are missing, implying that impurity phases were present in the composite at some point throughout the preparation process.[21].

Fourier-transform infrared spectroscopy (FTIR) Analysis

The composite's FTIR spectrum is displayed in

Fig. *02*. The transmittance peaks are 3918, 3878, 3838, 3752, 3687, 3473, 3416, 2828, 2851, 2092, 1636, 629, 475, and 421 cm^{-1}, respectively, according to the spectra. Table-2 shows the group frequencies attributed to their respective functional groupings.

Table-2: Showing different FTIR peaks.

Group frequency (cm^{-1})	Functional group/ions
405-565	Fe (II)-O stretching
705-575	Fe (II)-O stretching
1695-1595	CNT
2105-1705	Metal Carbonyl Transition
2945-2865	Methylene C-H symmetric stretching
2935-2915	Methylene C-H antisymmetric stretching
3575–3205	H-bonded OH stretching

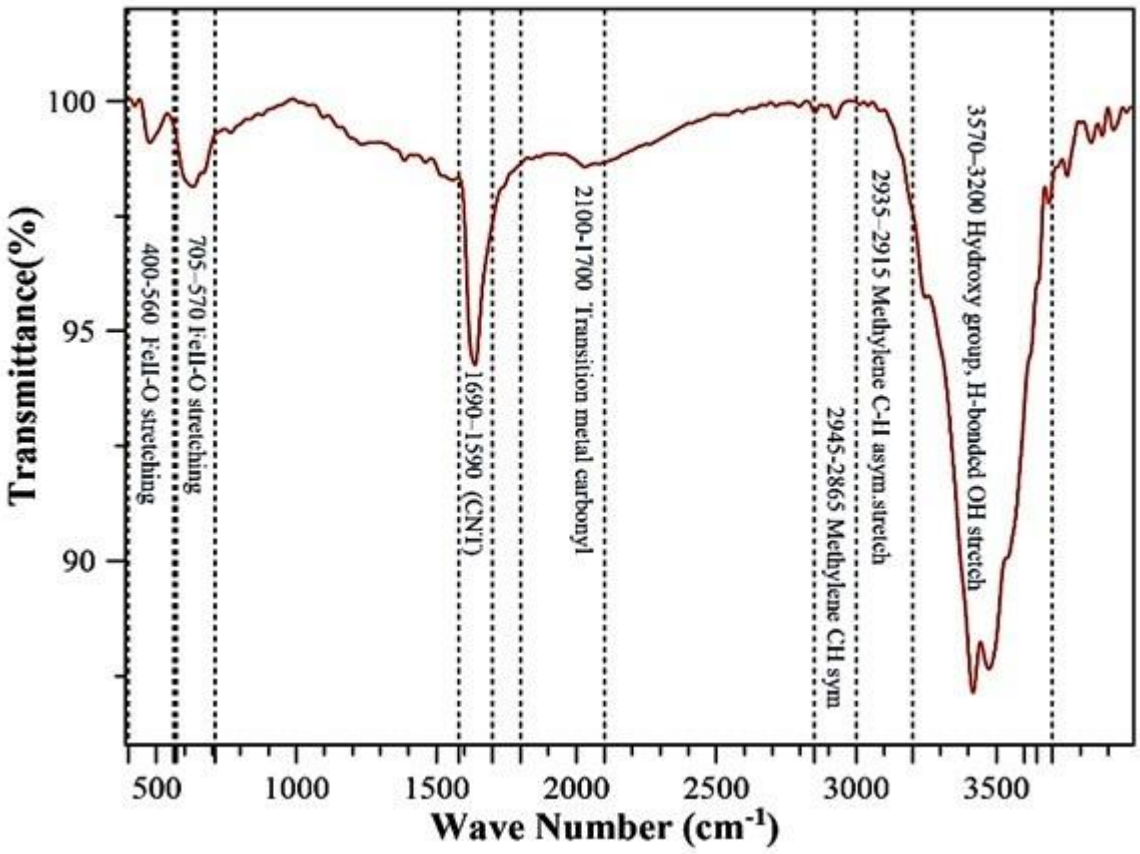

Fig. 02: FTIR peaks of nanohybrid showing presence of Iron and CNTs.

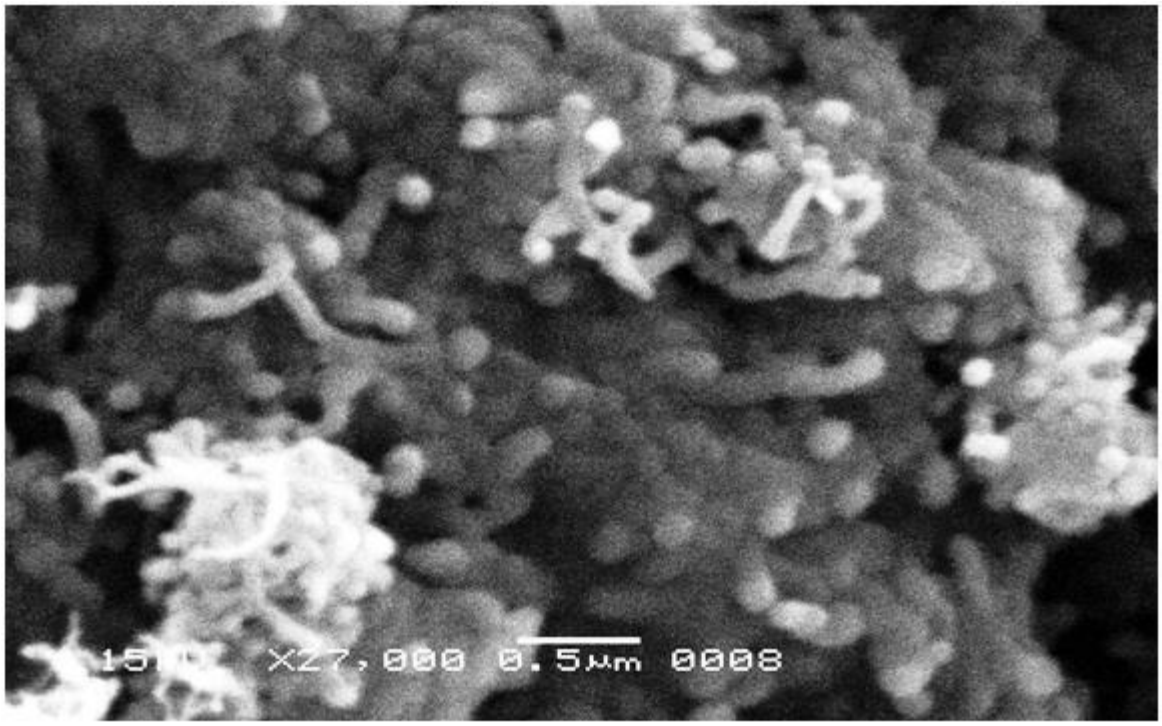

Fig. 03: SEM image captured at 500 nm and 27000 magnification.

Scanning Electron Microscope (SEM)

At various magnifications, SEM was utilized to evaluate the surface morphology. and scales.

Fig. *03* depicts hematite-like spheres painted on the surface of MWCNTs due to the hydrophobicity of CNTs, which are polycrystalline by nature due to the wet chemical method, and MWCNTs [25, 26]. Hematite causes aggregation of CNTs in the form of bundles and causes non-uniform dispersion of CNTs in the structure[26].

Energy Dispersive X-Ray (EDX) Analysis

The EDX standard, as shown in

Fig. *4*, confirms the purity and composition of the components of the combined hematite - MWCNT nanohybrids; where major peaks are around 0.8, 6.3, and 7.1 keV, which corresponds to the binding energies of Fe [27]. Only the components of Fe, O, C, and Pt are present in nanohybrids, according to EDX analysis[28], and the calculated atomic ratio of Fe to O is near to 2: 3, which is consistent with hematite's stoichiometric structure. The major components of hematite are Fe and O, and the Carbon peak belongs to MWCNT, while the height of Pt is attributable to platinum implantation during sample processing. **Error! Reference source not found.** shows the EDX elemental microanalysis (highest %) of nanohybrids.

Table-3: In EDX studies, the average weight and atomic percentages of elements were discovered.

Element	Weight percentage	Average	Atomic percentage	Average
C_1 (K)	66.43		89.24	
C_2 (K)	58.83	61.91	87.34	87.95
C_3 (K)	60.47		87.28	
O_1 (K)	7.08		7.14	
O_2 (K)	6.99	7.15	7.79	7.64
O_3 (K)	7.38		7.99	
Fe_1 (L)	6.94		2.01	
Fe_2 (L)	7.68	7.67	2.45	2.36
Fe_3 (L)	8.41		2.61	
Pt_1 (M)	19.54		1.62	

Pt_2 (M)	**26.5**	**23.26**	**2.42**	**2.05**
Pt_3 (M)	**23.74**		**2.11**	

Vibrating-Sample Magnetometer (VSM)

The magnetic properties of the created nanohybrids were investigated using a Vibrating Sample Magnetometer VSM. The applied magnetic field was 1.2 T to -1.2 T. The saturation magnetization (Ms), remnant magnetization (Mr), and coercivity (Hc) of the hematite/CNT nanocomposite were 1.2 (emu/g), 0.5 (emu/g), and 0.02 tesla (200 Oersted), respectively, as depicted in

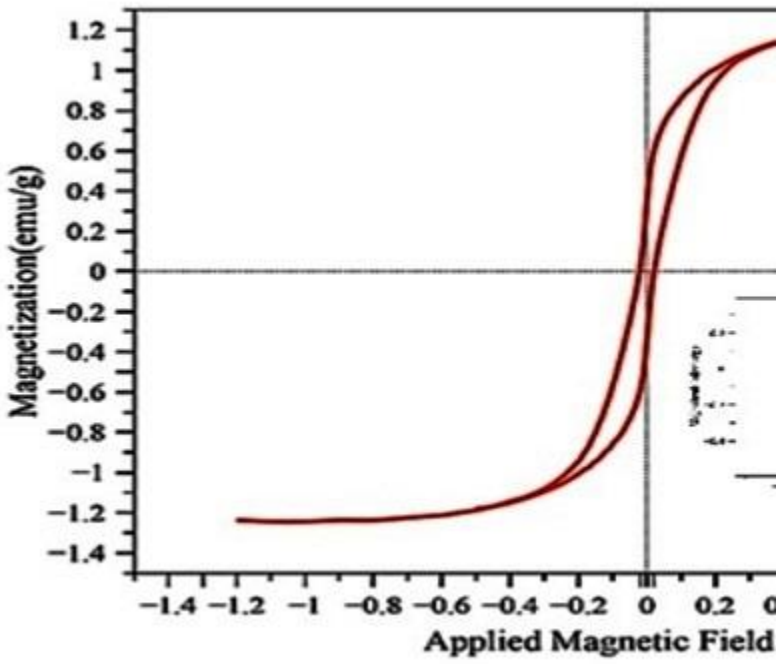

Fig 5.

Higher values of coercivity, saturation magnetization, and large magnetic susceptibility were observed in comparison to multiwalled CNTs, and the hybrid exhibits ferromagnetism [19, 25, 26], inferring small particle size with the high surface activity of hematite in comparison to bulk iron[29].

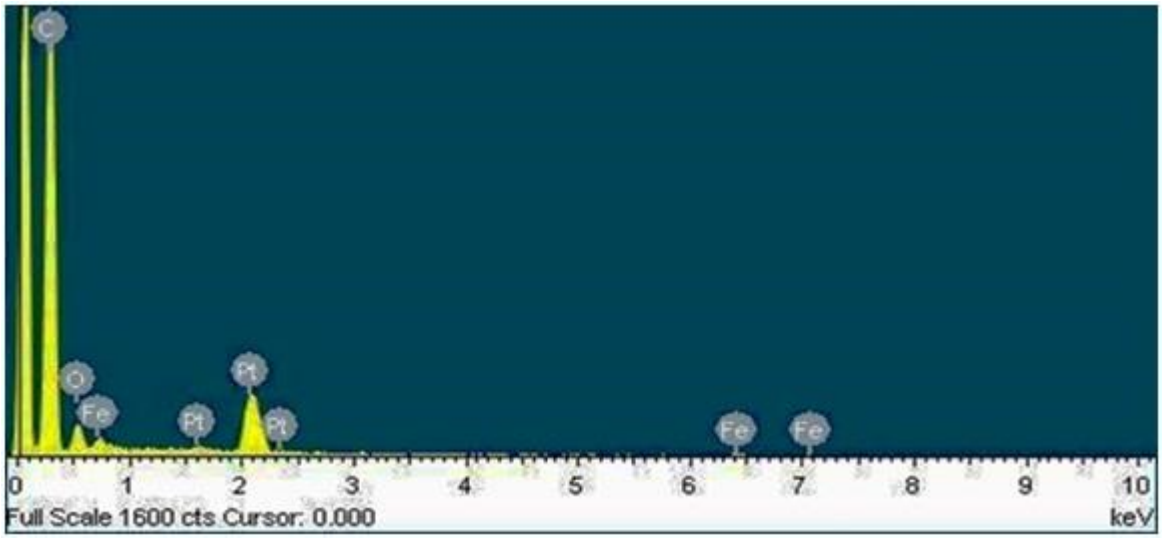

Fig. 4: EDX analysis of hematite – MWCNT nanohybrids.

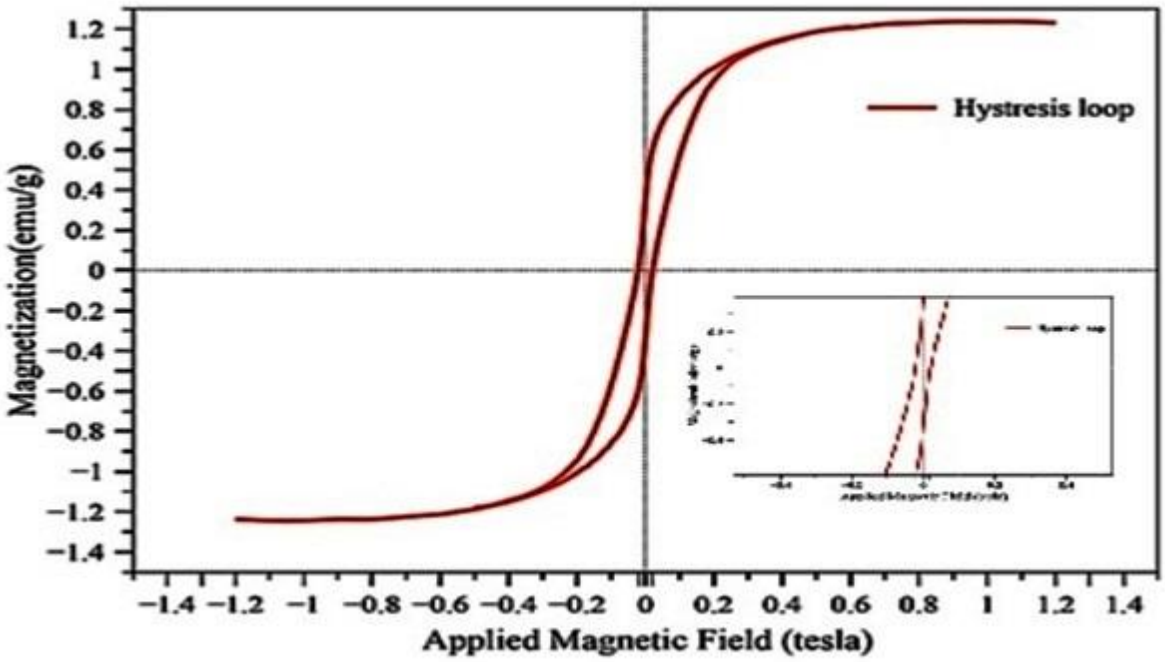

Fig 5: Shows the hysteresis loop and view of Nanohybrid when studied under VSM.

Conclusion

The presented wet method was found to be a cost-effective and repeatable nanohybrids synthetic method, which can be upgraded for a bulk production of metallic oxide nanohybrids. The economic integration of Hematite (approx. 26 nm) and MWCNTs; in the study will open a new door for modified surface morphologies that would subjugate the application of nanohybrids in various high-performance applications including energy storage and field emission-based devices. The fabricated nanohybrid is a promising anode electrode material for new generation Lithium-ion battery cells.

Acknowledgment

The authors are thankful to NEDUET, Karachi for moral support.

References

1. R. Zboril, M. Mashlan, and D. Petridis, Iron (III) oxides from thermal processes synthesis, structural and magnetic properties, Mössbauer spectroscopy characterization, and applications, *Chemistry of Materials*,**14**, 969 (2002).
2. H. Wang *et al.*, Comprehensive application of oolitic hematite for H2S removal at high temperature: performance and mechanism, *Energy and Fuels*, **33**, 2037 (2019).
3. M. Zhang, W. Luo, Z. Li, T. Yu, and Z. Zou, Improved photoelectrochemical responses of Si and Ti codoped α-Fe_2O_3 photoanode films, *Applied Physics Letters*, **97**, 042105 (2010).
4. A. Stein, Batteries take charge, *Nature Nanotechnology*, **6**, 262 (2011).
5. C. Pulgarin and J. Kiwi, Iron oxide-mediated degradation, photodegradation, and biodegradation of aminophenols, *Langmuir*, **11**, 519 (1995).
6. J. Chen, L. Xu, W. Li, and X. Gou, α-Fe2O3 nanotubes in gas sensor and lithium-ion battery applications, *Advanced Materials*, **17**, 582 (2005).
7. L. Camilli and M. Passacantando, Advances on sensors based on carbon nanotubes, *Chemosensors*, **6**, 62 (2018).
8. F. Zhao, H. Duan, W. Wang, and J. Wang, Synthesis and characterization of magnetic Fe/CNTs composites with controllable Fe nanoparticle concentration, *Physica B: Condensed Matter*, **407**, 2495 (2012).
9. D. Zhao, X. Wang, S. Yang, Z. Guo, and G. Sheng, Impact of water quality parameters on the sorption of U (VI) onto hematite, *Journal of environmental radioactivity*, **103**, 20 (2012).
10. C. Xu, X. Wang, and J. Zhu, Graphene− metal particle nanocomposites, *The Journal of Physical Chemistry C*, **112**, 19841 (2008).
11. S. F Hasany, N. H Abdurahman, and A. R Sunarti, Wet Chemical Approach for Vanadium Doped Maghemite (Fe2-xVxO3) Nanocrystals, *Current Nanoscience*,**12**, 617 (2016).
12. S.-L. Chou, J.-Z. Wang, Z.-X. Chen, H.-K. Liu, and S.-X. Dou, Hollow hematite nanosphere/carbon nanotube composite: mass production and its high-rate lithium storage properties, *Nanotechnology*, **22**, 265401 (2011).
13. D. Zhang, Z. Xu, Z. Yang, and X. Song, High-performance flexible self-powered tin disulfide nanoflowers/reduced graphene oxide nanohybrid-based humidity sensor driven by triboelectric nanogenerator, *Nano Energy*, **67**, 104251 (2020).
14. S. F. Hasany, N. Abdurahman, A. Sunarti, and A. Kumar, Non-covalent assembly of maghemite-multiwalled carbon nanotubes for efficient lead removal from aqueous solution, *Australian Journal of Chemistry*, **66**, 1440 (2013).
15. Z. Zhang *et al.*, Carbon nanotube/hematite core/shell nanowires on carbon cloth for supercapacitor anode with ultrahigh specific capacitance and superb cycling stability, *Chemical Engineering Journal*, **325**, 221 (2017).
16. J. M. George, A. Antony, and B. Mathew, Metal oxide nanoparticles in electrochemical sensing and biosensing: a review, *Microchimica Acta*, **185**, 1 (2018).
17. C. Xu *et al.*, Nature-inspired hierarchical materials for sensing and energy storage applications, *Chemical Society Reviews*, **50**, 4856 (2021).
18. C. Wang, K. Xia, H. Wang, X. Liang, Z. Yin, and Y. Zhang, Advanced carbon for flexible and wearable electronics, *Advanced materials*, **31**, 1801072 (2019).
19. M. Alaa, K. Yusoh, and S. Hasany, Synthesis and characterization of polyurethane–organoclay nanocomposites based on renewable castor oil polyols, *Polymer Bulletin*, **72**, 1 (2015).
20. N. N. Ghosh and A. B. Rajput, Preparation of polybenzoxazine-Ni-Zn ferrite nanocomposites and their magnetic property, in *Handbook of Benzoxazine Resins*: Elsevier, 641 (2011).
21. M. Krajewski *et al.*, Preparation and characterization of hematite-multiwall carbon nanotubes nanocomposite, *Journal of Superconductivity and Novel Magnetism*, **28**, 901 (2015).
22. J. Singh, M. Srivastava, J. Dutta, and P. Dutta, Preparation and properties of hybrid monodispersed magnetic α-Fe2O3 based chitosan nanocomposite film for industrial and biomedical applications, *International Journal of Biological Macromolecules*, **48**, 170 (2011).
23. S. Sahoo, K. Agarwal, A. Singh, B. Polke, and K. Raha, Characterization of γ-and α-Fe2O3 nano powders synthesized by emulsion precipitation-calcination route and rheological behaviour of α-Fe2O3, *International Journal of Engineering, Science and Technology*, **2** (2010).
24. M. Baibarac, I. Baltog, S. Lefrant, J. Mevellec, and O. Chauvet, Polyaniline and carbon nanotubes based composites containing whole units and fragments of nanotubes, *Chemistry of Materials*, **15**, 4149 (2003).

25. L. Jiang and L. Gao, Carbon nanotubes−magnetite nanocomposites from solvothermal processes: formation, characterization, and enhanced electrical properties, *Chemistry of materials*, **15**, 2848 (2003).
26. Z. Sun, Z. Liu, Y. Wang, B. Han, J. Du, and J. Zhang, Fabrication and characterization of magnetic carbon nanotube composites, *Journal of Materials Chemistry*, **15**, 4497 (2005).
27. L. Jiang and L. Gao, Carbon nanotubes−magnetite nanocomposites from solvothermal processes: formation, characterization, and enhanced electrical properties, *Chemistry of materials*, **15**, 2848 (2003).
28. F. Ren *et al.*, Lightweight and highly efficient electromagnetic wave-absorbing of 3D CNTs/GNS@ CoFe2O4 ternary composite aerogels, *Journal of Alloys and Compounds*,. **768**, 6 (2018).
29. M. B. Poudel, G. P. Awasthi, and H. J. Kim, Novel insight into the adsorption of Cr (VI) and Pb (II) ions by MOF derived Co-Al layered double hydroxide@ hematite nanorods on 3D porous carbon nanofiber network, *Chemical Engineering Journal*, **417**, 129312 (2021).